Co-published by
Institute of Fluid-Flow Machinery
Polish Academy of Sciences
Committee on Thermodynamics and Combustion
Polish Academy of Sciences

http://www.imp.gda.pl/archives-of-thermodynamics/

Experimental and numerical research on the impact of design solutions on the internal heat exchanger operating parameters

Jakub Janus[a*], Przemysław Skotniczny[a], Maria Richert[a], Jacek Długopolski[b]

[a]Strata Mechanics Research Institute, Polish Academy of Sciences, Reymonta 27, 30-059 Kraków, Poland
[b]AGH University of Science and Technology, Mickiewicza 30, 30-059 Kraków, Poland
*Corresponding author email: janus@imgpan.pl

Received: 25.03.2025; revised: 27.08.2025; accepted: 31.08.2025

Abstract

Research aimed at increasing the efficiency of heat exchangers used in car air conditioning systems may lead to modifications in the design of refrigeration systems. One such modification involves the use of smaller gas coolers, which directly reduces the overall production costs. This study presents an experimental investigation into the impact of constructional solutions on the performance of an internal heat exchanger using propylene glycol as a refrigerant. Two internal heat exchangers with different outer channel geometries were analysed. The experimental study was complemented by numerical simulations using the computational fluid dynamics method. The results showed that modifying the outer channel geometry from a parallel to a twisted configuration led to a 5.06% increase in cooling efficiency, a reduction of the outlet temperature by 2.2°C and a nearly 72 W increase in the total heat exchange rate. Numerical simulations confirmed the experimental findings, demonstrating good agreement with the measured data.

Keywords: Heat exchanger; IHX; Cooling efficiency; Numerical fluid mechanics; Numerical geometry

Vol. 46(2025), No. 4, 127–133; doi: 10.24425/ather.2025.156843

Cite this manuscript as: Janus, J., Skotniczny, P., Richert, M., & Długopolski, J. (2025). Experimental and numerical research on the impact of design solutions on the internal heat exchanger operating parameters. *Archives of Thermodynamics*, 46(4), 127–133.

1. Introduction

An internal heat exchanger (IHX) is a device that transfers heat between a high-pressure liquid stream and a low-pressure vapour stream. The liquid refrigerant exiting the condenser flows through the inner tube, while the vapour from the evaporator circulates in the outer channel. By lowering the temperature of the liquid before it enters the expansion devices, the IHX improves the overall performance of the refrigeration cycle.

With the progressive miniaturisation of refrigeration systems, improving the effectiveness of heat exchangers has become essential. This challenge has encouraged researchers to explore different approaches to enhance internal heat recovery. Methods include modifications of heat transfer mechanisms, the use of alternative refrigerants, and the redesign of exchanger geometry. Previous studies [1−5] demonstrated that altering the geometry of plate and internal heat exchangers can significantly improve heat transfer, enabling the development of more energy-efficient heating, ventilation and air conditioning (HVAC) systems. Similar solutions are increasingly applied in automotive refrigeration as well.

Figure 1 illustrates the layout of an automotive air-conditioning cycle. The installation comprises a compressor, a condenser and an evaporator connected in a closed refrigerant loop. After being compressed, the working fluid flows to the condenser, where it is cooled and condensed into liquid form with the assistance of forced air provided by fans. The liquid refrigerant then

Nomenclature

c_p – specific heat, J/(kg·K)
L – curve total length, m
q – total heat transfer rate, W
Q – mass flow rate, kg/s
r – cylinder radius, m
s – distance of the forming cylinder between the nearest points of the helix, m
t – parameter of moving alone the trajectory from 0 to 1
T – temperature, °C
y – Cartesian coordinate, m
z – Cartesian coordinate, position in the axis, m

Greek symbols

θ – rotation angle of the pull-out surface, deg
η – heat exchanger efficiency, %

Abbreviations and Acronyms

IHX – internal heat exchanger
CFD – computational fluid dynamics
FPGA– field programmable gate array

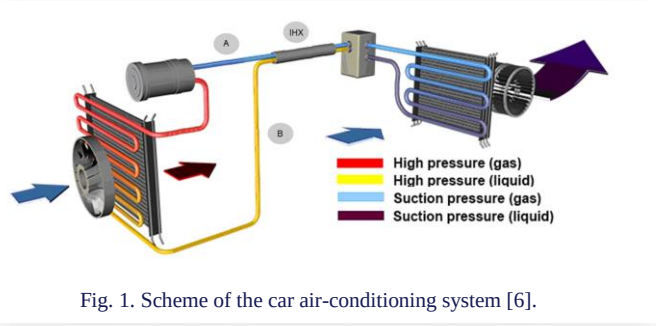

Fig. 1. Scheme of the car air-conditioning system [6].

passes through the IHX on its way to the evaporator, where a sharp temperature drop occurs during the expansion process. The function of the IHX is to improve system efficiency by transferring heat between the liquid stream in tube *B* and the colder vapour stream in tube *A*, thereby subcooling the liquid before expansion.

Recent studies also focus on innovative heat exchanger designs. Among the proposed solutions are the microjet configurations [6] and technologies based on mini- and microchannels [7,8]. These approaches enable a significant enhancement of the heat transfer coefficient within the exchanger.

Computational tools, particularly numerical simulations based on the finite volume methods (FVMs), have become a powerful instrument in heat exchanger research and design. Computational fluid dynamics (CFD) makes it possible to analyse complex processes, including flow behaviour, temperature field and stress distributions, even under challenging conditions, such as underground mining environments [9−12]. One of the key strengths of CFD is its ability to represent phenomena in both two- and three-dimensional domains. A comprehensive review of literature on CFD applications in the heat exchanger design is provided in [13], where the authors, after examining 66 publications, emphasised the cost-effectiveness and versatility of such simulations. They demonstrated that CFD can support the design process at various stages – from preliminary flow predictions to final optimisation of exchanger geometry. Numerical studies [2,14] apply CFD specifically to internal heat exchangers in refrigeration systems using CO_2, while other investigations address microchannel radiators in automotive air conditioning applications [15].

In recent years, significant progress has been made in the development of methods aimed at increasing the efficiency of heat transfer systems, particularly through the implementation of innovative designs, advanced simulations and the use of alternative working media. In [16], the use of machine learning was proposed for reconstructing multiphase fluid structures based on capacitive sensor data, showing the potential of intelligent diagnostics and control in thermal systems.

Experimental studies presented in [17] focused on the performance of a pumping engine in a micro organic Rankine cycle (micro-ORC) system utilising a low-boiling working fluid, demonstrating the influence of thermodynamic cycle design on the overall system efficiency. The study in [18] analysed the operation of a hybrid heating system based on heat pumps integrated with a photovoltaic installation, highlighting the growing role of renewable energy sources in thermal system optimisation.

In [19], a coupled heat, mass, and momentum transfer model was developed for a refrigerated storage chamber, providing valuable insights into the thermal behaviour of complex cooling environments. Furthermore, numerical simulations presented in [20] compared the effects of different baffle configurations in rectangular heat exchanger channels, confirming that modifications in internal geometry can significantly enhance heat transfer performance.

These studies emphasise the importance of combining experimental measurements with numerical modelling and intelligent analysis methods to design more efficient heat exchangers. The current research continues this trend by evaluating the impact of twisted outer channel geometry on the thermal efficiency of an internal heat exchanger operating with propylene glycol.

2. Geometry of internal heat exchangers and refrigerant selection

The simulations were performed for two tube-in-tube counterflow heat exchanger configurations, as illustrated in Fig. 2. In the first variant (model I), sixteen outer channels of the cooled medium were arranged in parallel to the central heating channel. In the second variant (model II), those outer channels were helically wound around the inner tube. In both variants, the exchanger design includes a central channel with a diameter of 16.4 mm, surrounded by sixteen outer channels. The cross-sectional shape and dimensions of these outer channels are presented in Fig. 3. Each considered heat exchanger type had an external radius of 12.5 mm and a total length of 1.0 m.

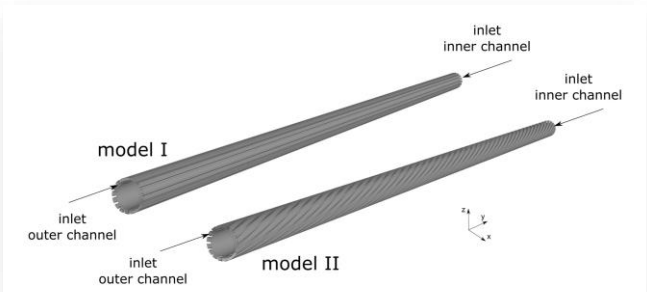

Fig. 2. Internal heat exchanger models.

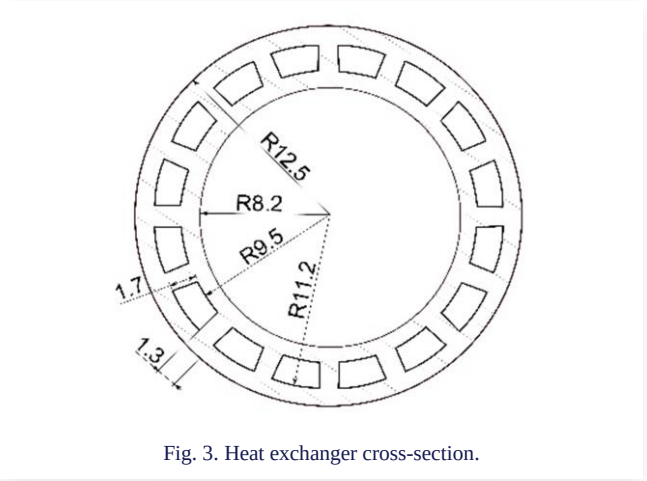

Fig. 3. Heat exchanger cross-section.

In model I, the outer channels were designed as straight prismatic channels. In contrast, model II employed helically wound outer channels, generated according to a parametric curve equation. The trajectory of this curve was implemented through a surface-extraction script in the pre-processing software:

$$s = 2\pi r \operatorname{ctg}(\theta), \tag{1}$$

$$\theta = \frac{L}{s} t \cdot 360, \tag{2}$$

$$z = tL, \tag{3}$$

where: s − distance of the forming cylinder between the nearest points of the helix, r – radius of the cylindrical surface defining the outer channel on which the helical trajectory is generated, θ − rotation angle of the pull-out surface, L − total length of the curve, t − parameter of moving alone the trajectory from 0 to 1, z − position in the axis.

The refrigerant used in research was the antifreeze propylene glycol InnovaTherm P/P-ALU (Table 1). It is an environmentally friendly liquid that is safe for humans. Additionally, it contains corrosion inhibitors for aluminium installations, extending their service life.

3. Laboratory research

The main purpose of laboratory tests [22] was to record the medium temperature at the inlet and outlet of the exchanger channels in various geometries. The assumptions for the laboratory station were to guarantee the possibility of testing the flow of liquid inside the IHX in the opposite direction.

Table 1. Selected properties of InnovaTherm P/P-ALU liquid [21].

Fluid	Crystallisation temperature (°C)	Boiling point (°C)	pH scale	Specific weight (kg/m³)	Dynamic viscosity at 20 °C (m Pa·s)	Thermal conductivity (W/(m K))
propylene glycol	–15	103	7.5–9.5	1020	3.15	0.457

To enable liquid temperature measurements in outer channels for both exchanger models, it was decided to use the connector, which was made by 3D printing technology. The connector is the end element of the exchanger, which directs the flow of liquid to the measuring point. Also, it performs a sealing function. Design of a measuring station is shown in Fig. 4. Thermostats with parameters shown in Table 2 were used as the source of heat and cold.

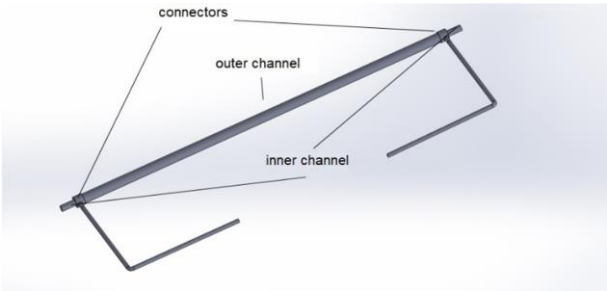

Fig. 4. Design of a measuring station.

Table 2. Parameters of thermostats.

Thermostat	Temperature range (°C)	Pump pressure (bar)	Max. pump flow (l/min)
Lauda A100	–20–100	0.4	17
Lauda WKL 1000	–10–40	1.0	30

The ends of the inner aluminium tube were threaded and then metal ends were placed at their ends to allow the system to be connected by a quick coupling system. Short conductive aluminium tubes were mounted on the ends of the outer tube to allow temperature reading. Temperature sensors were placed in selected locations. During the tests, the influence of external temperature on the measurements was limited by applying insulation foams.

To ensure the simultaneous temperature measurement at the inlet and outlet of the exchanger, it was decided to use digital DS18B20 temperature sensors produced by MAXIM-DALLAS Company. The temperature measurement range of the sensors was from – 55°C to 125°C, with a measurement accuracy declared by the manufacturer of 0.5%. A programmable system logic type FPGA (field programmable gate array) Cyclone III manufactured by INTEL Company [22] was used. The extension

of the laboratory station enabled testing of two internal heat exchangers simultaneously. Both stations were connected in parallel, which enabled testing both heat exchangers under the most similar conditions. The complex set is shown in Fig. 5. Operating parameters of the thermostats during laboratory test are presented in Table 3.

Fig. 5. Laboratory station for two internal heat exchangers (IHXs).

Table 3. Thermostat operating parameters during laboratory test.

Channel type	Pump flow (l/min)	Velocity (m/s)	Mass flow rate (kg/s)	Temperature (°C)
Inner channel	20	1.58	0.35	19.60
Outer channel	12	2.69	0.013	58.60

4. Numerical calculations

The next stage of research on the IHX cooling efficiency for various geometries was numerical tests using computational fluid dynamics. In order to obtain correct numerical calculation results, it was necessary to apply a dense calculation mesh. It was decided to use the mesh size function, which allows control of the size of the numerical mesh around the selected point, edge or surface [23]. A three-dimensional model of the internal heat exchanger was digitised with an unstructured tetrahedral mesh, which then, due to the large size of the model and selection of a dense computing mesh, was converted into a polyhedral mesh. The advantage of using this type of mesh is to obtain more accurate results by converting bad cells and obtaining the final results faster due to a smaller number of cells compared to the tetrahedral mesh. Mesh conversion was made using the Ansys Fluent 2020 software. The mesh consisted of 2.15 million elements for each geometric model. For numerical calculations, the k-ε turbulent model was used [23].

In the studied issue, there are two media: a liquid in the form of propylene glycol and a solid in the form of aluminium alloy. Their properties, presented in Table 4, were defined based on the Ansys Fluent software material database.

Boundary conditions for inner and outer channels were defined as a flat inlet velocity profile. The value of velocity was selected according to the pump flow parameters (Table 5).

Table 4. Properties of used materials.

Material	Density (kg/m³)	Thermal conductivity coefficient (W/(m·K))	Kinematic viscosity (kg/(m·s))	Specific heat (J/(kg·K))
Propylene glycol	1040	0.457	0.0157	2510
Aluminium alloy	2719	202.4	–	871

Table 5. Boundary conditions for numerical simulation.

Channel type	Pump flow (l/min)	Velocity (m/s)	Mass flow rate (kg/s)	Temperature (°C)
Inner channel	20	1.58	0.35	19.60
Outer channel	12	2.69	0.013	58.60

5. Results of laboratory tests and numerical calculations

The results of temperature measurements at the inlet and outlet of the channels in models I and II, carried out on a laboratory model, are presented as averaged temperature values from 30 measurement obtained after the temperature stabilisation, as shown in Tables 6 and 7, where: T_{R1} – refrigerant temperature at the hot inlet of the outer channel, T_{R1}'– refrigerant temperature at the hot outlet of the outer channel in model I, T_{R1}'' – refrigerant temperature at the hot outlet of the outer channel in model II, T_{R2} – refrigerant temperature at the cold inlet of the inner channel, T_{R2}' – refrigerant temperature at the cold outlet of the inner channel in model I, T_{R2}'' – refrigerant temperature at the cold outlet of the inner channel in model II.

The results of laboratory measurements allow us to notice changes in the temperature value at the outlet of the outer channel, caused by a change in the heat exchanger geometry. Twisting the outer channels, in which the heating medium flows, caused the decrease in temperature at the outlet by 2.2°C. The obtained temperature at the outlet of the outer channel in model I is 43.0°C (Table 6), in model II this temperature drops to 40.80°C (Table 7).

The results of numerical calculations of the refrigerant temperature distribution in models I and II of the IHX are presented

Table 6. Laboratory measurement results – refrigerant temperature at the inlet and outlet of model I channels.

Inner channel	Outer channel
cold inlet	**hot inlet**
T_{R2} = 19.60°C	T_{R1} = 58.60°C
cold outlet	**hot outlet**
T_{R2}' = 40.20°C	T_{R1}' = 43.00°C

Table 7. Laboratory measurement results – refrigerant temperature at the inlet and outlet of model II channels

Inner channel	Outer channel
cold inlet	**hot inlet**
T_{R2} = 19.60°C	T_{R1} = 58.60°C
cold outlet	**hot outlet**
T_{R2}'' = 39.20°C	T_{R1}'' = 40.80°C

in the temperature diagram in the inner and outer channels. In addition, the results are presented in the form of temperature contours. The initial flow parameters at the inlet of the inner channel, outer channel and calculated parameters at the outlet are presented in tabular form [24].

Figure 6 shows the temperature distribution at the exchanger cross-section y = 0 m. Due to the counter-current flow configuration, this plane corresponds to the inlet of the outer channel and the outlet of the inner channel. The figure illustrates the difference in refrigerant temperature between model I and model II. As the medium flows through the outer channels from y = 0 m to y = 1 m, the influence of the lower temperature in the inner channels becomes evident, leading to a reduction in the refrigerant temperature in the outer channel. At the outlet of the outer channel (y = 1 m), the influence of the twisted outer channels (model II) is noticeable, resulting in a lower refrigerant temperature compared to model I. The heating effect of refrigerant flowing through the inner channel in model II is slightly larger compared to model I. During the temperature contours analysis, a higher temperature of refrigerant was observed near the channel wall compared to the temperature in the central part of the channel cross-section (Fig. 7). This is due to the way of medium flows. During the fluid flow in closed channels, velocity and temperature profiles are created in subsequent cross-sections. The maximum value of velocity is located in the middle flow

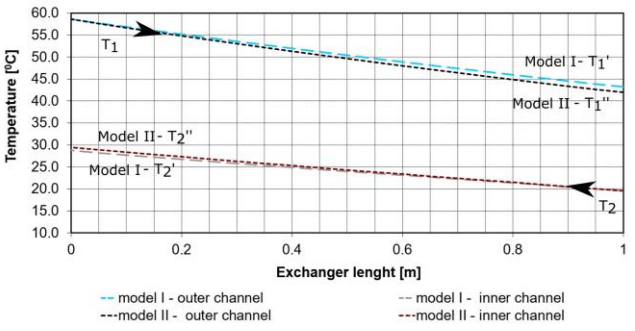

Fig. 6. Numerical simulation results − temperature distribution in the inner and outer channels.

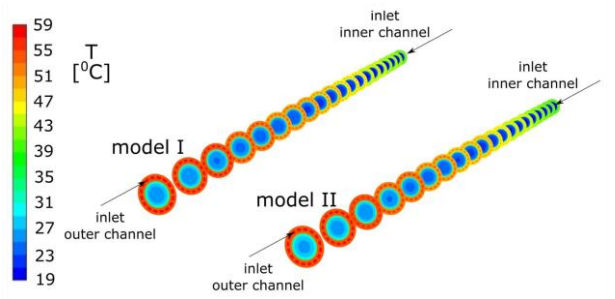

Fig. 7. Numerical simulation results − temperature contours for model I and II.

zone, which is a potential core, within which the lowest heat exchange occurs. For both models I and II, the biggest changes in temperature values occur at the end cross-section of the inner and outer channels. It is caused by the occurrence of the largest temperature gradient in these cross-sections.

The changes observed in the potential core flow region in the inner channel indicate an increase in the cooling effect in model II. These differences are visible in Tables 8 and 9, where: T_1 – refrigerant temperature at the hot inlet of the outer channel, T_1' – refrigerant temperature at the hot outlet of the outer channel in model I, T_1'' – refrigerant temperature at the hot outlet of the outer channel in model II, T_2 – refrigerant temperature at the cold inlet of the inner channel, T_2'– refrigerant temperature at the cold outlet of the inner channel in model I, T_2'' – refrigerant temperature at the cold outlet of the inner channel in model II. For the same boundary conditions, the difference in temperature obtained at the inner channel outlet between model I and model II is 0.64°C. In the outer channel, the temperature at the outlet decreased due to a geometry change from 43.23°C to 41.94°C.

The temperature distribution in the outer channel, obtained using the numerical method, corresponds to the temperature obtained during the laboratory test. For the same boundary conditions, at the outlet of the outer channel in model I, the measured temperature is 43.00°C, while the temperature obtained by the numerical method is 43.23°C. In the case of results for model II, the difference between the obtained results from numerical calculation and measurements increases to 1.14°C.

Table 8. Numerical calculation results – refrigerant temperature at the inlet and outlet of model I channels.

Inner channel	Outer channel
cold inlet	**hot inlet**
T_2 = 19.60°C	T_1 =58.60°C
cold outlet	**hot outlet**
T_2' = 28.81°C	T_1' = 43.23°C

Table 9. Numerical calculation results – refrigerant temperature at the inlet and outlet of model II channels.

Inner channel	Outer channel
cold inlet	**hot inlet**
T_2 = 19.60°C	T_1 = 58.60°C
cold outlet	**hot outlet**
T_2'' = 29.45°C	T_1'' = 41.94°C

Much larger discrepancies between the results of laboratory tests and numerical calculations were obtained for the inner channel. For model I, the measured temperature at the outlet of the inner channel is 40.20°C, while the temperature obtained by numerical calculations is 28.81°C. For model II, the measured temperature at the outlet of the inner channel is 39.20°C, while the numerical calculations show a temperature of 29.45°C.

Such significant differences in temperature indications for the inner channel can be caused by the temperature sensors' location in the channel cross-section. Analysing the graph in Fig. 8, which shows the temperature distribution in the inner channel cross-section in model II, the lower temperature (26.00°C) around the channel axis can be observed. However, near the inner channel wall, this temperature increases to around 55.00°C.

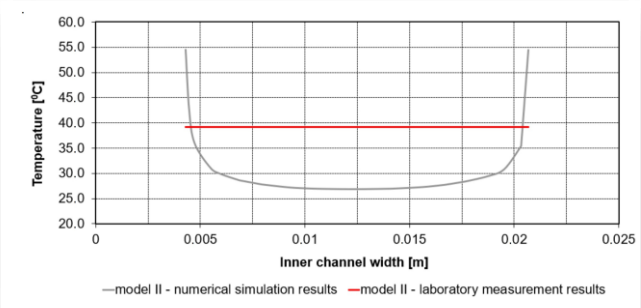

Fig. 8. Temperature distribution in the inner channel cross section, model II.

The temperature obtained from numerical simulations is the average temperature for the entire cross-section of the inner channel, while the measurement results indicate the temperature at one point in the cross-section. This temperature varies depending on the selection of the measuring point.

The heat exchanger efficiency for models I and II was calculated using the following formulas:

$$\begin{aligned} \eta_{RI} &= \frac{T_{R1}-T_{R1}'}{T_{R1}-T_{R2}} \cdot 100\%, \\ \eta_{RII} &= \frac{T_{R1}-T_{R1}''}{T_{R1}-T_{R2}} \cdot 100\%, \\ \eta_{I} &= \frac{T_{1}-T_{1}'}{T_{1}-T_{2}} \cdot 100\%, \\ \eta_{II} &= \frac{T_{1}-T_{1}'}{T_{1}-T_{2}} \cdot 100\%, \end{aligned} \tag{4}$$

where η_{RI} and η_{RII} are the heat exchanger efficiency for model I and model II, respectively, both calculated based on the laboratory measurements, and η_I and η_{II} represent the heat exchanger efficiency for model I and model II, respectively, calculated based on numerical simulation results.

The heat transfer rate may be obtained from the overall energy balance for the hot fluid. The total heat transfer rates for models I and II were calculated using the following formulas:

$$\begin{aligned} q_{RI} &= Q_m c_p \left(T_{R1} - T_{R1}'\right), \\ q_{RII} &= Q_m c_p \left(T_{R1} - T_{R1}''\right), \\ q_{I} &= Q_m c_p \left(T_{1} - T_{1}'\right), \\ q_{II} &= Q_m c_p \left(T_{1} - T_{1}''\right), \end{aligned} \tag{5}$$

where: Q_m = 0.013 kg/s, c_p = 2510 J/(kg·K); q_{RI} is the total heat transfer rate for model I, calculated based on laboratory measurements; q_{RII} − total heat transfer rate for model II, calculated based on laboratory measurements; q_I − total heat transfer rate for model I, calculated based on numerical calculation results; q_{II} − total heat transfer rate for model II, calculated based on numerical calculation results.

The calculated heat exchanger efficiency and total heat transfer rate are presented in Table 10, where: RI – results of laboratory measurements for model I, RII – results of laboratory measurements for model II, I – results of numerical calculations for model I, II – results of numerical calculations for model II.

Table 10. Summary of the calculated exchanger efficiency and total heat transfer rate for model I and II.

	Heat exchanger efficiency (%)	Total heat transfer rate (W)
RI	40.00	509.03
RII	45.06	580.81
I	39.41	501.52
II	42.74	543.62

The results show that the changes in geometry of the heat exchanger outer channels increase the efficiency of heat exchange by 5.06%. This efficiency was calculated based on laboratory measurements. As regards the numerical simulation results, the difference in the calculated efficiency between models I and II was 3.33%.

For the operating conditions presented above, the calculated heat transfer rate based on laboratory measurements is 509.03 W for model I and 580.81 W for model II. In the case of numerical simulation, the calculated heat transfer is equal to 501.52 W for model I and 543.62 W for model II.

4. Conclusions

This paper presents the results of laboratory tests and numerical simulations investigating the impact of constructional modifications on the cooling efficiency of an internal heat exchanger using propylene glycol as a refrigerant. Two heat exchanger models with different outer channel geometries were designed and analysed. In model I, the outer channels were arranged parallel to the inner channels, while in model II, the outer channels were helically twisted around the inner channel.

The experimental results indicate that modifying the geometry of the outer channels led to a 5.06% increase in cooling efficiency when compared to the conventional parallel design. This improvement is attributed to the elongation of the outer channels, which enhanced the heat exchange surface area and improved thermal performance. Additionally, the modification resulted in a 2.2°C lower temperature at the inner channel outlet, further demonstrating the effectiveness of the twisted-channel configuration. The total heat exchange rate also increased by nearly 72 W, which translates into improved efficiency of the car air conditioning system.

The findings from laboratory tests were further validated through numerical simulations, which provided a detailed representation of heat transfer characteristics in both models. The numerical calculations closely aligned with the experimental results, confirming the reliability of the applied methodology. The boundary conditions used in the simulations were consistent with laboratory assumptions, ensuring the accuracy of the computational models.

These results highlight the potential benefits of implementing twisted outer channel designs in heat exchangers for automotive applications. By enhancing heat transfer performance, such modifications contribute to the development of more efficient and cost-effective refrigeration systems, reducing energy consumption and improving overall system reliability.

Acknowledgements

This paper is financed from the statutory funds of the Strata Mechanics Research Institute of the Polish Academy of Sciences.

References

[1] Furberg, R., Palm, B., Li, S., Toprak, M., & Muhammed, M. (2009). The use of a nano- and microporous surface layer to enhance boiling in a plate heat exchanger. *Journal of Heat Transfer*, 131(10), 101010. doi: 10.1115/1.3180702

[2] Sanchez, D., Patino, J., Llopis, R., Cabello, R., Torrella, E., & Fuentes, F.V. (2014). New positions for an internal heat exchanger in a CO_2 supercritical refrigeration plant: Experimental analysis and energetic evaluation. *Applied Thermal Engineering*, 63(1), 129–139. doi: 10.1016/j.applthermaleng.2013.10.061

[3] Wajs, J., & Mikielewicz, D. (2014). Effect of surface roughness on thermal-hydraulic characteristics of a plate heat exchanger. *Key Engineering Materials*, 597, 63–74. doi: 10.4028/www.scientific.net/KEM.597.63

[4] Wajs, J., & Mikielewicz, D. (2016). Influence of a metallic porous microlayer on pressure drop and heat transfer of a stainless steel plate heat exchanger. *Applied Thermal Engineering*, 93, 1337–1346. doi: 10.1016/j.applthermaleng.2015.08.101

[5] Zhang, F.Z., Jiang, P.X., Lin, Y.S., & Zhang, Y.W. (2011). Efficiencies of subcritical and transcritical CO_2 inverse cycles with and without an internal heat exchanger. *Applied Thermal Engineering*, 31(4), 432–438. doi: 10.1016/j.applthermaleng.2010.09.018

[6] Wajs, J., Mikielewicz, D., Fornalik-Wajs, E., & Bajor, M. (2015). Recuperator with microjet technology as a proposal for heat recovery from low-temperature sources. *Archives of Thermodynamics*, 36(4), 49–64. doi: 0.1515/aoter-2015-0032

[7] Mikielewicz, D., & Wajs, J. (2017). Possibilities of heat transfer augmentation in heat exchangers with minichannels for marine applications. *Polish Maritime Research*, 24(s1), 133–140. doi: 10.1515/pomr-2017-0031

[8] Rahman, M.M., Kariya, K., & Miyara, A. (2018). An experimental study and development of new correlation for condensation heat transfer coefficient of refrigerant inside a multiport minichannel with and without fins. *International Journal of Heat and Mass Transfer*, 116, 50–60. doi: 10.1016/j.ijheatmasstransfer.2017.09.010

[9] Dziurzyński, W., Pałka, T., & Krach, A. (2014). Computer simulation of the propagation of heat in abandoned workings insulated with slurries and mineral substances. *Archives of Mining Sciences*, 59(1), 3–23. doi: 10.2478/amsc-2014-0001

[10] Janus, J., & Krawczyk, J. (2017). Modeling of the propagation of methane from the longwall goaf, performed by means of a two-dimensional description. *Archives of Mining Sciences*, 59(4), 851–868. doi: 10.2478/amsc-2014-0059

[11] Janus, J., & Krawczyk, J. (2014). The numerical simulation of a sudden inflow of methane into the end segment of a longwall with Y-type ventilation system. *Archives of Mining Sciences*, 59(4), 941–957. doi: 10.2478/amsc-2014-0065.

[12] Śliwa, T., Gołaś, A., Wołoszyn, J., & Gonet, A. (2012). Numerical model of borehole heat exchanger in Ansys CFX software. *Archives of Mining Sciences*, 57(2), 375–390. doi: 10.2478/v10267-012-0024-3

[13] Mahmood, M., Bhutta, A., Hayat, N., Bashir, M.H., Khan, A.R., Ahmad, K.N., & Khan, S. (2012). CFD applications in various heat exchanger designs: A review. *Applied Thermal Engineering*, 32, 1–12. doi: 10.1016/j.applthermaleng.2011.09.001

[14] Ituna-Yudonago, J.F., Belman-Flores, J.M., Elizalde-Blancas, F., & García-Valladares, O. (2017). Numerical investigation of CO_2 behavior in the internal heat exchanger under variable boundary conditions of the transcritical refrigeration system. *Applied Thermal Engineering*, 115, 1063–1078. doi: 10.1016/j.applthermaleng.2017.01.042

[15] Janus, J., Skotniczny, P., & Richert, M. (2019). Modeling of the impact of construction solutions on operating parameters of the internal heat exchanger with refrigerant R744. *Archives of Thermodynamics*, 40(1), 145–160. doi: 10.24425/ather.2019.128295

[16] Ornowski, R., Lackowski, M., & Kwidzinski, R. (2024). Application of machine learning for reconstruction of multiphase fluid structure measured by a capacitance multi-electrode sensor. *Archives of Thermodynamics*, 45(4), 5–12. doi: 10.24425/ather.2024.151993

[17] Kaczmarczyk, T.Z. (2024). Experimental research of a pumping engine in a micro-ORC system with a low-boiling medium. *Archives of Thermodynamics*, 45(4), 125–140. doi: 10.24425/ather.2024.152002

[18] Turoń, M.K. (2024). Operation of a hybrid heating system based on heat pumps using a photovoltaic installation. *Archives of Thermodynamics*, 45(4), 153–162. doi: 10.24425/ather.2024.152004

[19] Kołodziejczyk, M., Śmierciew, K., & Gagan, J., Butrymowicz, D., Jakończuk, P., Pawłowski, M. (2024). Coupled heat, mass and momentum transfer model of a napa cabbage refrigerated storage chamber. *Archives of Thermodynamics*, 45(4), 223–235. doi: 10.24425/ather.2024.152012

[20] Zidani, C., Benyoucef, B., Didi, F., & Guendouz, N. (2020). Simulation and numerical analysis of a rectangular pipe with transversal baffle – comparison between zigzag and plane baffles. *Archives of Thermodynamics*, 41(4), 269–283. doi: 10.24425/ather.2020.135988

[21] http://innova-therm.pl/zabezpieczenie-przed-zamarzaniem/innova-therm-p--p-alu.html [accessed 24 March 2025].

[22] Długopolski, J., & Richert, M. (2019). Naturally parallel measuring system based on FPGA hardware. *Journal of Machine Construction and Maintenance*, 113(2), 113–119.

[23] Ansys Inc. (2016). *Ansys Fluent Users Guide*.

[24] Li, M.J., Zhang, H., Zhang, J., Mu, Y.T., Tian, E., Dan, D., Zhang, X.D., & Tao, W.Q. (2018). Experimental and numerical study and comparison of performance for wavy fin and a plain fin with radiantly arranged winglets around each channel in fin-and-channel heat exchangers. *Applied Thermal Engineering*, 133, 298–307. doi: 10.1016/j.applthermaleng.2018.01.01